ACS APPLIED MATERIALS & INTERFACES

Research Article

www.acsami.org

High Mobility of Graphene-Based Flexible Transparent Field Effect Transistors Doped with TiO_2 and Nitrogen-Doped TiO_2

Yu-Hsien Wu, Po-Yuan Tseng, Ping-Yen Hsieh, Hung-Tao Chou, and Nyan-Hwa Tai*

Department of Materials Science and Engineering, National Tsing-Hua University, No. 101, Sec. 2, Kuang-Fu Road, Hsin-chu 30013, Taiwan

Supporting Information

ABSTRACT: Graphene with carbon atoms bonded in a honeycomb lattice can be tailored by doping various species to alter the electrical properties of the graphene for fabricating p-type or n-type field-effect transistors (FETs). In this study, large-area and single-layer graphene was grown on electropolished Cu foil using the thermal chemical vapor deposition method; the graphene was then transferred onto a poly(ethylene terephthalate) (PET) substrate to produce flexible, transparent FETs. TiO_2 and nitrogen-doped TiO_2 (N-TiO_2) nanoparticles were doped on the graphene to alter its electrical properties, thereby enhancing the carrier mobility and enabling the transistors to sense UV and visible light optically. The results indicated that the electron mobility of the graphene was 1900 $cm^2/(V{\cdot}s)$. Dopings of TiO_2 and N-doped TiO_2 (1.4 at. % N) lead to n-type doping effects demonstrating extremely high carrier mobilities of 53000 and 31000 $cm^2/(V{\cdot}s)$, respectively. Through UV and visible light irradiation, TiO_2 and N-TiO_2 generated electrons and holes; the generated electrons transferred to graphene channels, causing the FETs to exhibit n-type electric behavior. In addition, the Dirac points of the graphene recovered to their original state within 5 min, confirming that the graphene-based FETs were photosensitive to UV and visible light. In a bending state with a radius of curvature greater than 2.0 cm, the carrier mobilities of the FETs did not substantially change, demonstrating the application possibility of the fabricated graphene-based FETs in photosensors.

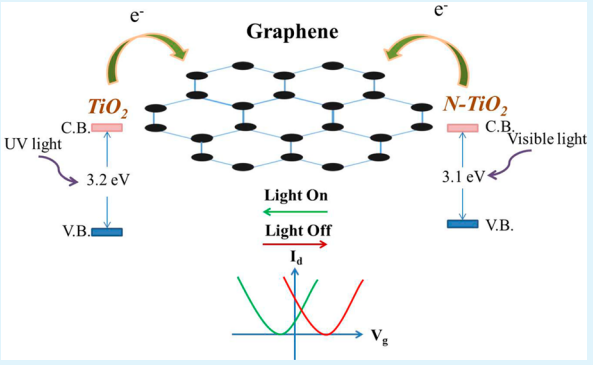

KEYWORDS: *graphene FET, transparent, flexible, titanium dioxide, nitrogen-doped titanium dioxide, high mobility*

INTRODUCTION

Graphene, a monolayered carbon material with a hexagonal structure, is regarded as a promising material in many applications because of its unique optoelectrical properties, superior chemical stability and mechanical properties, and extremely high carrier mobility. According to theoretical predictions, graphene has an extraordinary carrier mobility of up to 200000, which is obviously higher than that of a silicon thin-film transistor (Si-TFT) having a value lower than 10;[1−5] therefore, it is considered to be a promising material for next-generation electronic devices. In addition, as a result of its high transmittance property, graphene has a high potential application in flexible transparent electronics.

Because of the remarkable properties of graphene, graphene-based FETs exhibit ambipolar characteristics; thus, tuning the properties of doped-graphene-based FETs allows them to behave as n-type or p-type, which is highly competitive with the present electronic devices. Doping is an effective approach to tailoring the electrical properties of devices performing n-type or p-type behaviors. Two types of doping, surface-transfer doping and substitutional doping, are generally employed.[6] The former involves electron exchange between graphene and dopants because graphene has a high surface area/volume ratio and easily absorbs atoms, gas molecules, and ionic compounds.[7,8] The latter results from the replacement of the carbon atoms in the graphene network by dopants, which creates hole acceptors or electron donors, depending on the dopants. As a consequence, the Fermi level is changed, and consequently, the band gap at the Dirac point of graphene is opened.[9−12] Because substitutional doping can distort the graphene lattice and degrade the carrier mobilities, we chose to use surface-transfer doping.

In this study, we fabricated flexible transparent graphene thin-film transistors (G-FETs) doped with TiO_2 and nitrogen-doped TiO_2 (N-TiO_2) and studied the effects of the dopants on the electrical properties of the G-FETs. The advantages of using TiO_2 as a dopant include the following: (1) TiO_2 has a lower work function than graphene,[13,14] thus causing the transfer of electrons from TiO_2 to graphene and leading to an n-type doping effect. (2) When exposed to UV light, TiO_2 can generate electrons and holes, with the electrons being able to transfer from TiO_2 to graphene, causing a more significant n-type doping effect. (3) The photoactive properties of TiO_2 can be modulated by modifying TiO_2 (for example, nitrogen-doped

Received: January 1, 2015
Accepted: April 23, 2015
Published: April 23, 2015

DOI: 10.1021/am508996r
ACS Appl. Mater. Interfaces 2015, 7, 9453−9461

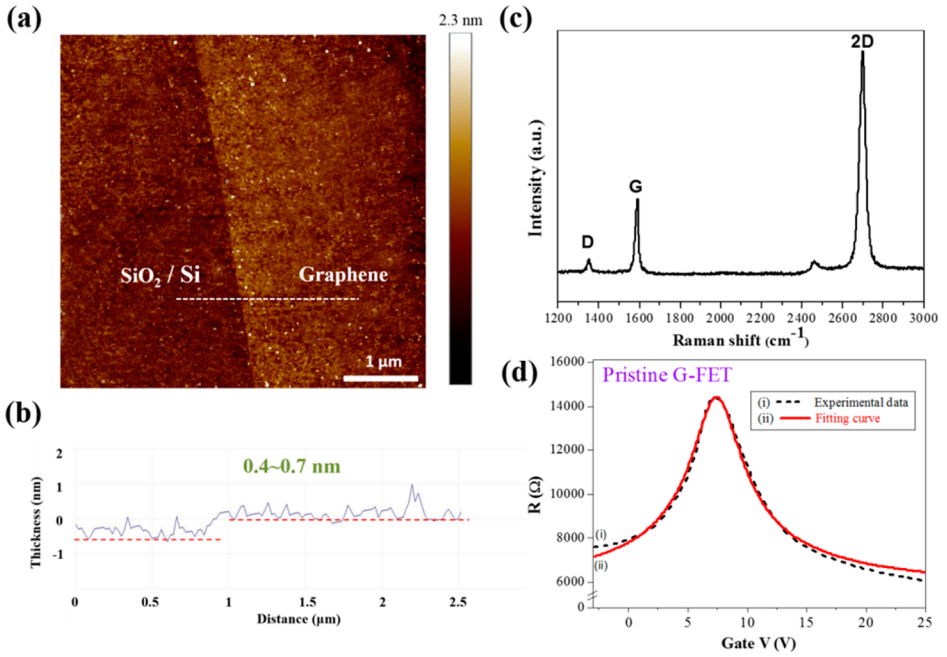

Figure 1. (a) AFM image, (b) height profile corresponding to the white dotted line in panel a, (c) Raman spectrum of graphene transferred from electropolished Cu foil to the SiO_2/Si substrate, and (d) $R-V_G$ curve of pristine G-FET (V_D = 0.01 V) (black symbols and solid red line represent experimental data and fitted curve, respectively).

TiO_2 can cause a reduction in the band gap, so that N-TiO_2 is photosensitive to visible light instead of UV light);[15] therefore, it is expected that the n-type doping effect of graphene can be accomplished by applying visible light. (4) TiO_2 is inexpensive and nontoxic.

To the best of our knowledge, only a few works have reported the electric behaviors of TiO_2-doped G-FETs,[16] and nearly no studies have investigated N-TiO_2 doping, especially for flexible transparent FETs. Comparisons of the electrical properties of G-FETs without TiO_2 doping and with TiO_2 and N-TiO_2 dopings were made. The electrical properties of TiO_2 and N-TiO_2 G-FETs were measured under irradiation of UV and visible light, respectively. In addition, bending tests to demonstrate the flexibility of the fabricated devices were also performed, and the results are discussed.

METHODS

Graphene and G-FETs. In our previous study, single-layer graphene was synthesized on an electropolished Cu foil by the chemical vapor deposition (CVD) method, and G-FETs were fabricated using a lithography process with poly(ethylene terephthalate) (PET) as the substrate.[17] In contrast to our previous work, we used poly(vinyl alcohol) (PVA) as the dielectric-layer material in this study instead of poly(methyl methacrylate) (PMMA) because PVA has a higher dielectric constant than PMMA (8.15 and 4.22, respectively; Table S1, Supporting Information). In the processing of G-FETs, the source and drain electrodes (chromium and gold, 20 and 40 nm, respectively) were first prepared by the lithography and lift-off processes. After the graphene had been transferred to the plastic substrate, graphene channels were patterned by the secondary lithography and O_2 plasma etching processes. The quality of the graphene before the lithography and after the etching process was examined by Raman spectroscopy, and no significant degradation was found (Figures S1 and S2, Supporting Information). Subsequently, spin-coating with a PVA solution followed by a baking process at 130 °C for 1 h was applied to prepare the PVA dielectric layer. The top gate electrodes (Au) with a thickness of 100 nm were deposited by sputtering using a patterned mask. Optical microscopy (OM) images of the G-FET and an image of the graphene channel can be found in Figure S3 (Supporting Information).

TiO_2 Nanosol and N-TiO_2 Nanoparticles. A TiO_2 nanosol was synthesized through the processes of hydrolysis and peptization in a titanium isopropoxide (TTIP, supplied by Aldrich) solution.[13,44] TTIP (4 mL), isopropanol (12 mL, supplied by J. T. Baker), and distilled water (200 mL) were homogeneously mixed, and white precipitates immediately formed from the hydrolysis reaction. The precipitate solution was ultrasonicated, and the pH was adjusted to 1.5 using nitric acid (supplied by Sigma-Aldrich). The solution was then heated to 80 °C for 48 h to achieve the peptization reaction. Finally, the solution was filtered through a cellulose acetate membrane filter with a pore size of 200 nm. In preparing the N-TiO_2 nanoparticles, TiO_2 nanoparticles (P25, supplied by Degussa) were heated at three temperatures (500, 600, and 700 °C) in an ammonia atmosphere for 4 h.[45] After the reaction, the N-TiO_2 nanoparticles were homogeneously dispersed in distilled water for the subsequent graphene doping process. The concentrations of TiO_2 nanosol and N-TiO_2 solution were both 2.5 mg/mL.

Doping of TiO_2 and N-TiO_2 on Graphene and Fabrication of G-FETs. An additional spin-coating process was applied for both the TiO_2 and N-TiO_2 G-FETs after being processed in the graphene channel, although it was not applied in the fabrication of G-FETs. The TiO_2 nanosol and N-TiO_2 solution were dropped onto the graphene channel for the preparation of TiO_2 and N-TiO_2 G-FETs, respectively. The spinning was performed for 30 s at the four spin rates of 500, 400, 300, and 200 rpm. The devices were then dried at 70 °C for 1 h to remove the solvent, after which the dielectric layer and top gate electrode were fabricated.

Raman Spectroscopy Characterization. Graphene films transferred onto 300-nm SiO_2/Si substrates was examined using a Raman spectrometer equipped with a 514.2-nm laser (Horiba Jobin Yvon HR 800 UV instrument with a 100× objective).

Atomic Force Microscopy. Graphene films transferred onto 300-nm SiO_2/Si substrates were examined by atomic force microscopy (AFM; Bruker Dimension ICON). The thickness of the graphene was measured in tapping mode under the ambient atmosphere.

FET Mobility Measurements. Electrical properties of the FET devices were measured with a semiconductor parameter analyzer (4200-SCS, Keithley) at room temperature under the ambient

DOI: 10.1021/am508996r
ACS Appl. Mater. Interfaces 2015, 7, 9453−9461

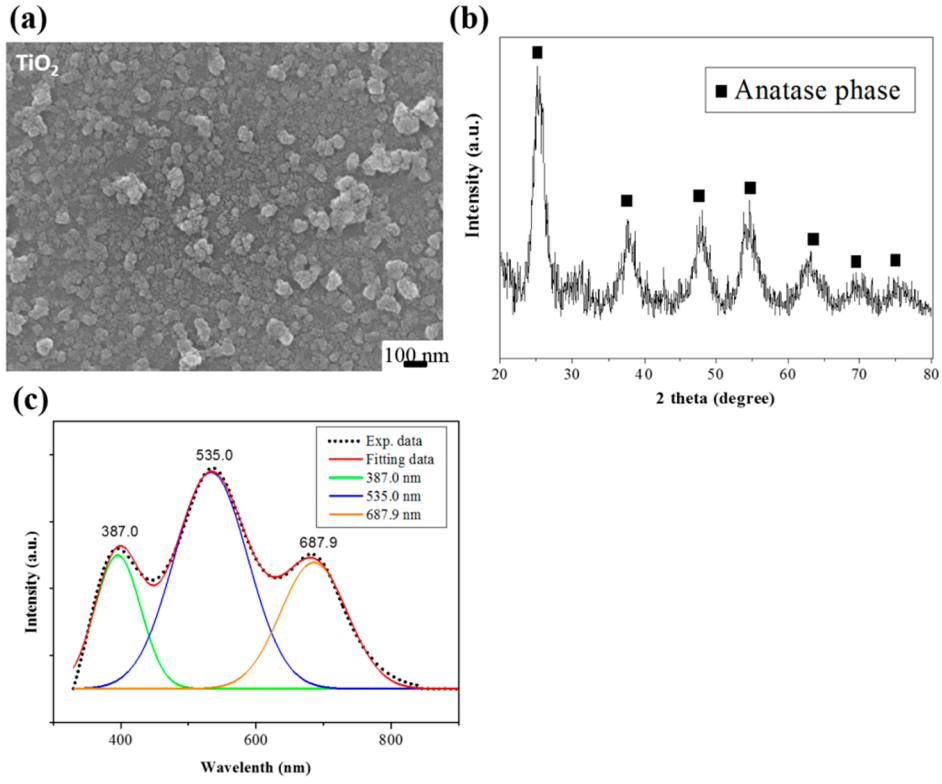

Figure 2. (a) SEM image, (b) XRD pattern, and (c) PL spectrum of TiO_2 nanoparticles.

atmosphere. Based on the plots of the drain current (I_D) as a function of the gate voltage (V_G) for the FET devices at a specific drain voltage (V_D), the carrier mobilities and on/off ratios were determined.

RESULTS AND DISCUSSION

In this work, we used electropolished Cu foil as a substrate for graphene deposition because it was reported that treated Cu foil can improve the quality of the synthesized graphene.[17] Before fabricating the flexible transparent G-FETs, we transferred graphene from the electropolished Cu foil to a SiO_2/Si (300 nm) substrate to characterize the morphology and quality of the synthesized graphene. The thickness of the graphene was measured by atomic force microscopy (AFM). As shown in Figure 1a, a border between the SiO_2/Si substrate (left) and the graphene (right) is evident; the graphene thickness can be estimated from the difference in height between the graphene and the SiO_2/Si substrate. The corresponding thickness profile shown in Figure 1b indicates that the graphene thickness was 0.4−0.7 nm, which is slightly greater than that of an ideal single layer of graphene (0.34 nm). The difference was likely due to the adsorption of water molecules onto the graphene surface, resulting in an increased thickness of the single-layer graphene with a typical thickness of 0.6−1.0 nm. The measurement of the thickness of the as-fabricated graphene was performed in the ambient atmosphere rather than in a high-vacuum environment; therefore, the adhesion of water molecules onto the graphene was unavoidable. In this regard, Albrektsen et al. mentioned the same point of view.[18] Moreover, the interactions of the AFM tip with graphene and SiO_2 are different, causing variations in the measurement.[19−21] Giannazzo et al. reported that the surface topography of a coating layer can be precisely obtained only if the substrate is covered with the same coating material.[21] A similar phenomenon was also reported in the measurement of WO_3 nanoparticles.[22]

Three characteristic peaks in the Raman spectrum for graphene are the D band (1250−1350 cm^{-1}), the G band (1580−1600 cm^{-1}), and the 2D band (2650−2700 cm^{-1}), indicating defects in the graphene structure, the E_{2g} vibration mode of sp^2-bonded carbon, and a second-order two-phonon process, respectively. The intensity ratio of the 2D band to the G band (I_{2D}/I_G) was higher than 1.5, indicating single-layer graphene.[23−27] The Raman spectrum of the graphene on a SiO_2/Si substrate is presented in Figure 1c, showing a high I_{2D}/I_G ratio greater than 2.0 and a low I_D value. Both the calculation of the I_{2D}/I_G ratio from the Raman spectrum and the thickness determined using AFM suggested that high-quality single-layer graphene was prepared. All electrical measurements were performed using a semiconductor parameter analyzer with probe stations. Figure 1d shows the $R-V_G$ curve (where R is resistance) of a pristine G-FET. The Dirac point (DP) was 7.4 V, which was slightly higher than the ideal value (0 V), because of the p-type doping of graphene due to the absorption of water molecules from the atmosphere.[7,28] The total resistance of an FET can be expressed as[29,30]

$$R_{total} = \frac{L_{ch}}{W_{ch}} R_c + \frac{L_{ch}}{W_{ch} e \mu \sqrt{{n_0}^2 + {n_G}^2}} \quad (1)$$

where R_c is the electrode metal/graphene contact resistance; L_{ch} (15 μm) and W_{ch} (10 μm) are the length and width, respectively, of the graphene channel; e and μ are the electron charge and carrier mobility, respectively; and n_0 and n_G represent the residual carrier concentration and the carrier concentration induced by the gate bias, respectively. The value of n_G was obtained using the equation

$$n_G = \frac{C_G(V_G - V_{G,Dirac})}{e} \quad (2)$$

DOI: 10.1021/am508996r
ACS Appl. Mater. Interfaces 2015, 7, 9453−9461

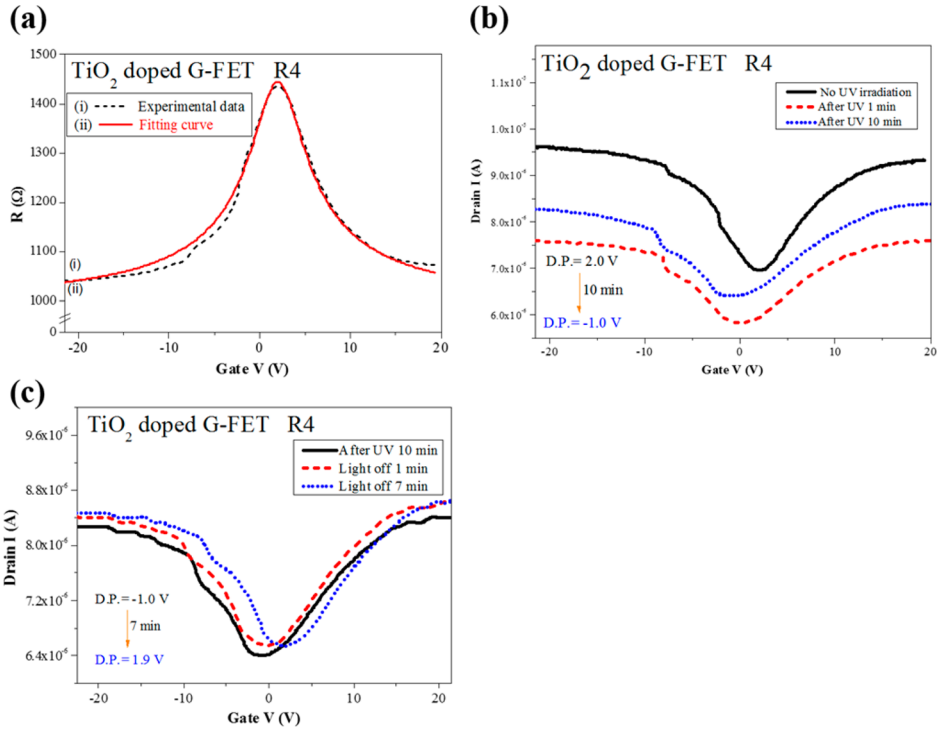

Figure 3. (a) $R-V_G$ curve of TiO_2-doped G-FET R4 (V_D = 0.01 V) (black symbols and solid red line represent experimental data and a fitted curve, respectively). (b,c) Changes in I_D-V_G curves of TiO_2-doped G-FET R4 (b) after exposure to UV irradiation for various times and (c) for various times after the UV light was turned off.

where C_G (~4.1 × 10^{-8} F/cm^2) is the sheet capacitance of the dielectric layer determined by capacitance−voltage ($C-V$) measurements.

Figure 1d shows the experimental data (black symbols) and the curve fitted according to the theoretical model expressed in eq 1 (red solid line), enabling the values of R_c, μ, and n_0 to be extracted. R_c and n_0 were estimated to be approximately 3050 Ω and 6.2 × 10^{11} cm^{-2}, respectively, for holes and 2500 Ω and 7.8 × 10^{11} cm^{-2}, respectively, for electrons. The carrier mobility μ was found to be 2400 $cm^2/(V\cdot s)$ for holes and 1900 $cm^2/(V\cdot s)$ for electrons. These values are higher than those of a top-gated flexible G-FET [$\mu_h \approx 260$ $cm^2/(V\cdot s)$ and $\mu_e \approx 140$ $cm^2/(V\cdot s)$].[31] The improvement in carrier mobility might be associated with a reduction of Columbic scattering. Similar work was performed by Kim et al., who used ion gel as the dielectric and attributed the enhancement in mobility to capturing charges and neutralizing the trapped charges, which could result in Columbic scattering.[31] Because PVA contains abundant hydroxyl groups, PVA can neutralize trapped charged impurities on the substrate, thereby increasing the carrier mobility. The yield of the pristine G-FET process was approximately 75%. (The Dirac points of 11 devices were detected from 14 as-fabricated devices from the last batch.)

A scanning electron microscopy (SEM; JEOL JSM-6500F) image of TiO_2 nanoparticles with diameters in the range of 40−80 nm is presented in Figure 2a. The TiO_2 was characterized as the anatase phase, as confirmed by the X-ray diffraction (XRD; Shimadzu 6000) pattern in Figure 2b. The photoluminescence (PL; Perkin-Elmer LS 55) spectrum was measured in the full wavelength range from 300 to 900 nm and was fitted according to Lorentz curve fitting, as shown in Figure 2c. Three primary peaks at 387.0, 535.0, and 687.9 nm were found, corresponding to a small amount of reflected source radiation, recombination of a mobile electron with a trapped hole on the TiO_2 surface, and the second order of the 387.0-nm peak, respectively.[32] The peak at 387.0 nm corresponds to a band gap of 3.2 eV, indicating that TiO_2 can be irradiated using UV light.

During the graphene doping process, the TiO_2 nanosol was spin-coated onto the graphene channels for 30 s at three spinning speeds: 500 rpm (R5), 400 rpm (R4), and 300 rpm (R3). The results obtained from R4 were the most favorable among these three conditions (Figure 3a). After doping of the graphene with the TiO_2 nanosol, the DP shifted toward negative voltages because of the n-type doping (the DP of 7.4 V for the undoped G-FET was shifted to 2.3, 2.0, and 1.9 V for R5, R4, and R3, respectively). These results can be explained by the difference in the work functions of TiO_2 (4.0 eV) and graphene (4.42 eV),[13,14] which enabled electron transfer from TiO_2 to graphene. The lower spin-coating speed resulted in a higher doping concentration, leading to a greater DP shift.

The electron transfer resulted in positively charged impurities on the TiO_2 surface; these impurities acted as a source of an additional electric field effect for the charged carriers in the graphene, resulting in an increased electron mobility.[13,33] Based on the $R-V_G$ curve, the extracted electron mobilities of R5, R4, and R3 were 5200, 27000, and 53000 $cm^2/(V\cdot s)$, respectively, indicating that the electron mobility of the graphene was greatly improved by TiO_2 doping. Regarding the mobilities, several published articles have demonstrated that high mobilities are possible depending on the doping materials, dielectric layer, measuring environment, and so on.[34−38] In addition, mobility models also affect the calculated mobilities. High mobilities of ~60000 $cm^2/(V\cdot s)$ for a suspended graphene FET in liquids with various dielectric materials have been reported.[34]

In our work, TiO_2 was used as the dopant, and enhanced carrier mobilities were observed. These results can be attributed to the following reasons: (1) The electron transfer results in

DOI: 10.1021/am508996r
ACS Appl. Mater. Interfaces 2015, 7, 9453−9461

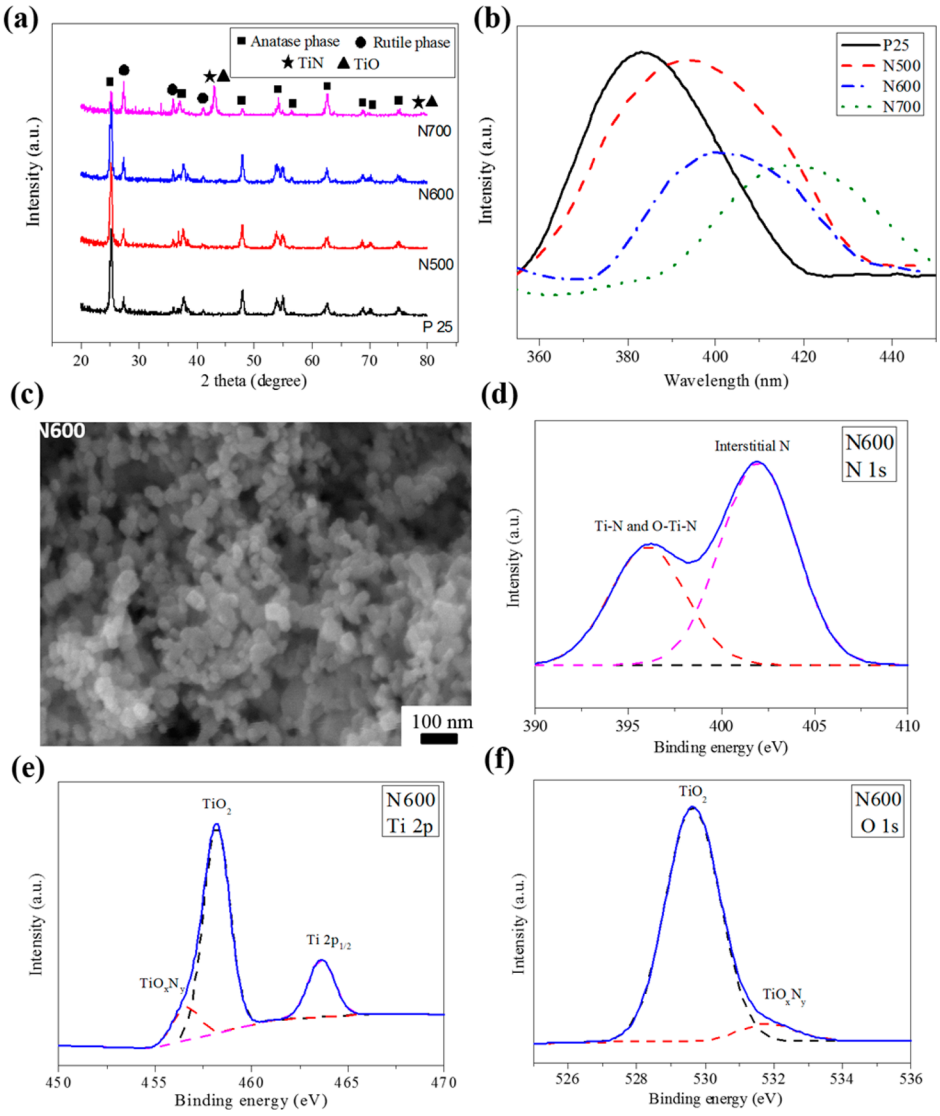

Figure 4. (a) XRD patterns, (b) PL spectra, and (c) SEM image (only N600) of P25 and N-TiO_2 nanoparticles. (d–f) ESCA spectra of N600 in the binding energy regions of (d) N 1s, (e) Ti 2p, and (f) O 1s core levels.

positively charged impurities on the TiO_2 surface, which act as an additional electric field for charge carriers in the graphene.[13] (2) A screening effect suppresses the mobility degradation due to long-range scattering of charged impurities.[39] (3) Extra electrons were provided due to oxygen vacancies in TiO_x, which was treated at relatively low temperature (80 °C).[16] TiO_x is a high-dielectric material with the dielectric constant of 70–120,[40] consequently enhancing the carrier mobility.

It was expected that higher electron mobilities could be achieved when a lower spinning speed was employed; however, spinning speeds lower than 300 rpm produced a nonuniform coating of TiO_2 nanosol on the graphene channel, resulting in irregular $R-V_G$ curves. The yield of TiO_2-doped G-FETs was 70%; this yield was slightly lower than that of pristine G-FETs because of the additional doping process.

The electrical properties of TiO_2-doped G-FETs subjected to UV irradiation were measured. Figure 3b shows the transfer curves of R4. We found that the DPs shifted toward negative voltages under UV irradiation but remained unchanged after a number of minutes. The DP of R5 shifted from 2.3 V (before UV irradiation) to 0.4 V (after 10 min of UV irradiation); similar results were observed for R4, whose DP shifted from 2.0 to −1.0 V (after 10 min), and for R3, whose DP shifted from 1.9 to −1.8 V (after 5 min). The DP of R3 shifted most significantly within the shortest length of time, because R3 had the highest doping concentration. Interestingly, the graphene channels of R4 and R3 were converted from p-type to n-type after UV irradiation. The DP shift was regarded as the transfer of photogenerated electrons from the surface of TiO_2 to the graphene channels.

After the variation in DP had stabilized, the UV light was turned off, and the electrical properties were measured. Figure 3c shows the changes in the DP of R4 after the UV light was turned off. The results indicate that the DPs tended to recover to their initial states within a certain number of minutes and the became graphene channels p-type semiconductors. The DPs of R5, R4, and R3 recovered from 0.4 to 2.3 V (after 3 min), from −1.0 to 1.9 V (after 7 min), and from −1.8 to 1.1 V (after 10 min), respectively. A possible reason for the recovery of the DPs is that the photogenerated electrons could react with oxygen or moisture trapped in the graphene channel, thus causing electron neutralization and reducing the n-type doping

DOI: 10.1021/am508996r
ACS Appl. Mater. Interfaces 2015, 7, 9453–9461

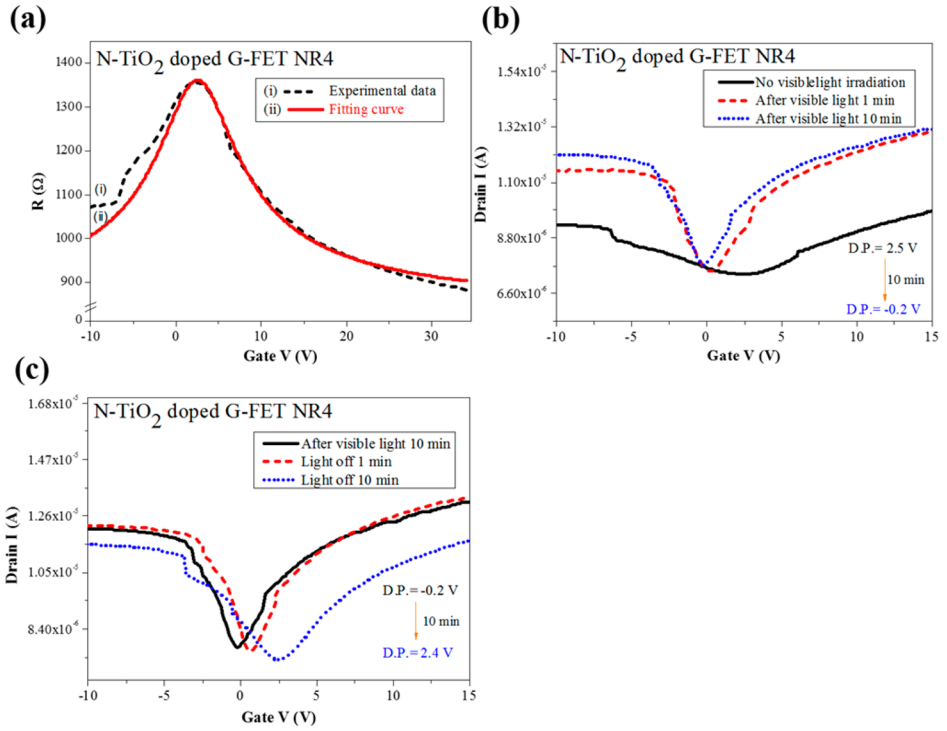

Figure 5. (a) $R-V_G$ curve of N-TiO_2-doped G-FET NR4 (V_D = 0.01 V) (black symbols and solid red line represent experimental data and a fitted curve, respectively). (b,c) Changes in I_D-V_G curves of N-TiO_2-doped G-FET NR4 (b) after exposure to visible light irradiation for various times and (c) for various times after the visible light was turned off.

effect.[13] The behaviors of the DP shift and recovery exhibited characteristics of optical sensing. These results reveal that the extent of DP recovery increased with increasing spinning speed. The recovery percentages of R5, R4, and R3 were 100% (returned to its original state), 97%, and 78%, respectively. This might be because the n-doping effect of R5 (the lowest doping amount) was more easily reduced than that of R3 (the highest doping amount).

Although R3 exhibited the highest electron mobility, the transfer properties of R4 were more suitable for an optically sensing FET, because the DP could recover to its initial state and the material return to a p-type semiconductor after UV irradiation was terminated.

The n-type doping of the G-FETs could be obtained when the graphene channels were doped with N-TiO_2 nanoparticles, which were prepared by heating P25 at three temperatures, namely, 500 °C (N500), 600 °C (N600), and 700 °C (N700), in an ammonia atmosphere. As shown in Figure 4a, the XRD patterns of P25 and the three types of N-TiO_2 suggest that the primary phases were anatase and rutile. With increasing reaction temperature, the intensity of the anatase peak located at 2θ = 25.4° tended to decrease, whereas the intensity of the rutile peak located at 2θ = 27.5° increased. This phase change is related to the lattice transformation of TiO_2, which occurs at approximately 600−700 °C.[41] Furthermore, the XRD pattern of N700 includes diffraction peaks corresponding to TiO and TiN, indicating that parts of the TiO_2 were converted to titanium oxynitrides, TiO_xN_y,[42] which is likely due to the higher nitrogen content of N700 compared to N500 and N600 in the reaction of P25 and ammonia at elevated temperatures. No TiO and TiN diffraction peaks were found for N500 and N600. Regarding changes in the band gap, nitrogen doping caused shifts in the PL peak from 383.5 nm (P25) to 393.5 nm (N500), 400 nm (N600), and 417.5 nm (N700), corresponding to band gaps of 3.2, 3.15, 3.1, and 2.97 eV, respectively, as shown in Figure 4b. Interestingly, N600 and N700 presented a shift in photocatalytic activity from the UV to the visible light range. Therefore, N700 and N600 were more appropriate than N500 for graphene doping. The band-gap reduction is attributed to the fact that the band gap of N (2p) is lower than that of O (2p) and the substitution of nitrogen atoms in oxygen sites leads to a decrease in the band gap of TiO_2 after nitrogen doping.[43]

The morphology variation of N-TiO_2 under different temperature treatments was also examined. Coalescence sintering of N-TiO_2 was observed for N700, which might have affected the uniformity of subsequent doping on graphene. Instead, the particle coalescence of N600 was not as severe as that of N700, as shown in Figure 4c; therefore, we used N600 as a dopant. The chemical bonding of N600 was investigated using electron spectroscopy for chemical analysis (ESCA; Ulvac-PHI PHI 1600), as shown in Figure 4d−f. The N 1s peak is known to be at binding energies of 396.0−396.9 and 401.1 eV for substitutional N atoms and interstitial N atoms, respectively.[15] For Ti $2p_{3/2}$ bonding, peaks at 454.7−455.1 eV, 456.0−456.7 eV, and 458.1−458.3 eV should be assigned to TiN, TiO_xN_y, and TiO_2, respectively. O 1s bonding peaks at 530.2 and 531.8 eV can be assigned to TiO_2 and TiO_xN_y, respectively.[42] Our results for N600 revealed the presence of Ti−N and O−Ti−N bonds, indicating that some nitrogen atoms were bonded to Ti; interstitial N atoms were also observed in the N 1s peak at 401 eV because N atoms were in the lattice space of TiO_2. Moreover, both the Ti $2p_{3/2}$ and O 1s spectra also provided evidence of the bonding of Ti and N because of the presence of the TiO_2 and TiO_xN_y peaks. Nevertheless, no Ti−N bonding was observed in the Ti $2p_{3/2}$ spectrum, possibly because of a lower nitrogen content. Using ESCA, we estimated the elementary contents as follows: 43.0

DOI: 10.1021/am508996r
ACS Appl. Mater. Interfaces 2015, 7, 9453−9461

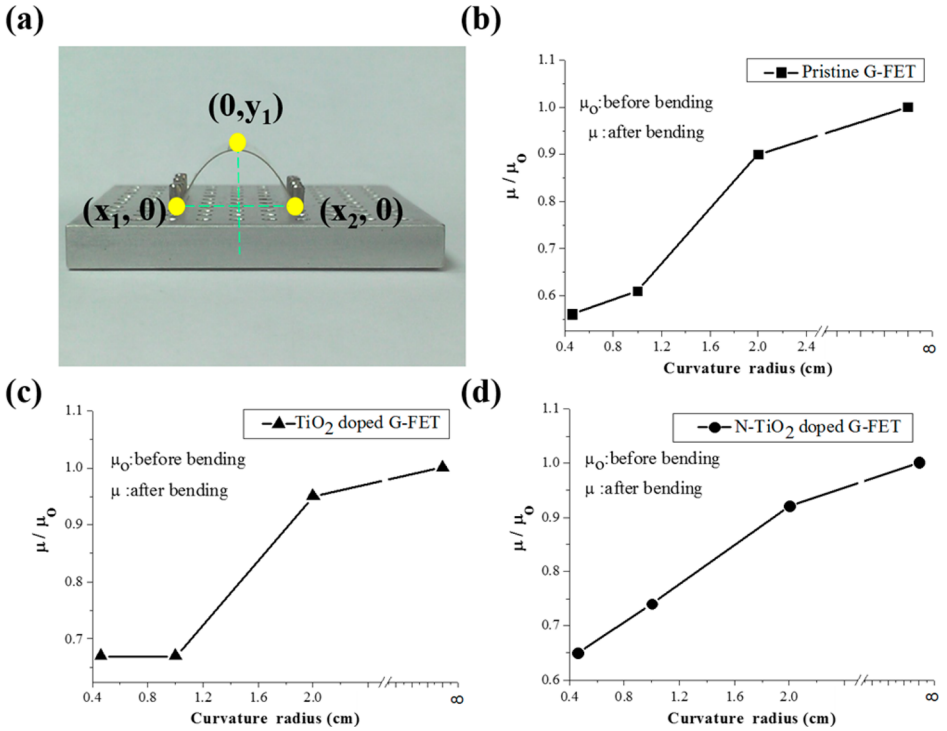

Figure 6. (a) Schemeatic of the bending test. (b–d) Variations of the carrier mobility at different curvature radii for (b) pristine graphene, (c) TiO_2-doped graphene, and (d) N-TiO_2-doped graphene.

at. % Ti, 56.4 at. % O, and 0.06 at. % N for N500; 48.4 at. % Ti, 50.2 at. % O, and 1.4 at. % N for N600; and 57.3 at. % Ti, 36.6 at. % O, and 6.1 at. % N for N700.

The process for doping N-TiO_2 (N600) on graphene was similar to that of doping TiO_2, with the denotations NR5, NR4, and NR3 representing the three spinning speeds of 500, 400, and 300 rpm, respectively. Figure 5a shows the results obtained from NR4, which were the most favorable among these three conditions. As expected, the electrons on N-TiO_2 tended to transfer to graphene after the doping and caused the DPs to shift toward negative voltages (the DP of graphene was 7.4 V and shifted to 3.2, 2.5, and 2.3 V after the doping of NR5, NR4, and NR3, respectively). As stated, lower spinning speeds resulted in a higher doping concentration and caused greater DP shifts. The extracted electron mobilities based on the $R-V_G$ curves of NR5, NR4, and NR3 were 3700, 21000, and 31000 $cm^2/(V{\cdot}s)$, respectively. The phenomenon of higher electron mobility with lower spinning speeds in N-TiO_2 doping was similar to that in TiO_2 doping. In addition, to obtain uniform doping, the lowest spinning speed of 300 rpm was used, and a yield of 70% was obtained for the N-TiO_2-doped G-FETs.

The electrical properties of N-TiO_2-doped G-FETs under visible light were measured. Figure 5b shows the transfer curves of NR4. The results show that, after visible light irradiation, the DP shifted toward negative voltages and remained unchanged after a number of minutes. The DPs of NR5, NR4, and NR3 shifted from 3.2 to 1.5 V (after 10 min), from 2.5 to −0.2 V (after 10 min), and from 2.3 to −1.1 V (after 7 min), respectively. The DP of NR3 shifted more significantly than the others because of the higher doping concentration. Similarly to TiO_2-doped G-FETs R4 and R3, the graphene channels of NR4 and NR3 were converted from p-type to n-type. The photogenerated electrons transferred from N-TiO_2 to the graphene channels, resulting in an n-type doping effect.

Recovery of the DPs of the N-TiO_2-doped G-FETs was achieved. N-TiO_2 could not continuously maintain graphene photogenerated electrons without irradiation of visible light; therefore, the DPs returned to their original states when the visible light was turned off, and the N-TiO_2-doped G-FETs reverted to a p-type semiconductor behavior. Figure 5c shows the variation in the DP of NR4 after the visible light was turned off. The DPs of NR5, NR4, and NR3 recovered from 1.5 to 3.2 V (after 5 min), from −0.2 to 2.4 V (after 10 min), and from −1.1 to 1.7 V (after 10 min), respectively. The recovery of the DP and the reduction in n-type doping intensity were due to neutralization of the photogenerated electrons by oxygen or moisture.[13] We found that the devices exhibited characteristics of optical sensing because of the shift and recovery of the DPs. The recovery percentages of the DPs of NR5, NR4, and NR3 were 100%, 96%, and 82%, respectively. The extent of DP recovery was associated with the doping amount, which was consistent with the results of TiO_2 doping. The transfer properties of both NR4 and NR3 were converted from p-type to n-type under visible light; however, NR4 was more suitable for visible light sensing because it reverted to a p-type semiconductor with higher recovery than NR3, although NR3 exhibited the highest electron mobility.

Concerning the flexibility of the G-FETs, the carrier mobilities of the devices under different radii of curvature were measured to demonstrate the flexibility of the G-FETs. Figure 6a illustrates the fixture for the bending test, in which the bending curve was assumed to be a parabolic curve and the radius of curvature was evaluated using the equations

$$y = ax^2 + bx + c \tag{3}$$

$$\text{radius of curvature} = \frac{1}{|2a|} \tag{4}$$

DOI: 10.1021/am508996r
ACS Appl. Mater. Interfaces 2015, 7, 9453–9461

Three types of graphene FETs (pristine, TiO_2, and N-TiO_2) showed similar variations in carrier mobility, as illustrated in Figure 6b–d, where μ_0 and μ are the carrier mobilities of the graphene FET before and after the bending process, respectively. We found that the μ_0/μ ratios of these three FETs decreased within 10% when we used a radius of curvature of 2.0 cm. Even under conditions of very extreme bending, with a radius of the curvature of 0.45 cm, the μ_0/μ ratios of these three FETs decreased within 50%. This demonstrates that the graphene channels were not significantly damaged when subjected to high tensile stress. Interestingly, the carrier mobilities were not substantially affected by bending when the radius of curvature was higher than 2.0 cm. In summary, the results confirmed that the G-FET and two types of doped G-FETs fabricated on PET substrates had great flexibility and exhibited excellent properties under a radius of curvature of 2.0 cm.

CONCLUSIONS

Flexible, transparent, and photosensitive top-gated G-FETs of high carrier mobility were successfully fabricated using dopings of TiO_2 and N-TiO_2. We found that nitrogen doping could induce a visible light response of TiO_2 and that the optimal nitrogen content of N-TiO_2 nanoparticles was 1.4 at. %. For the pristine G-FET, the carrier mobility and DP were 1900 $cm^2/(V{\cdot}s)$ and 7.4 V, respectively. Doping with TiO_2 and N-TiO_2 markedly enhanced the carrier mobility of graphene to 53000 and 31000 $cm^2/(V{\cdot}s)$, respectively, and shifted the DP of graphene to 1.9 and 2.7 V, respectively, indicating an n-type doping effect. Under exposure to UV and visible light, the doped G-FETs exhibited n-type transfer properties; without irradiation, these types of devices returned to their original states (from n-type to p-type). The DPs recovered to their initial states, indicating the photosensitive properties of these two types of doped FETs when exposed to UV and visible light. In the bending tests, the carrier mobilities of the bent pristine G-FET and two types of doped G-FETs were not substantially changed when they were subjected to a radius of curvature higher than 2.0 cm. In addition, the devices also exhibited FET characteristics, even under extreme bending conditions, with a radius of curvature lower than 0.45 cm, demonstrating the high flexibility of the fabricated doped G-FETs.

ASSOCIATED CONTENT

Supporting Information

Detailed fabrication process of flexible transparent top-gate G-FET device along with a schematic diagram (Figure S1). Raman spectra of graphene before and after the lithography process, demonstrating that the graphene was not destroyed during the lithography process (Figure S2). OM images of G-FET and image of the graphene channel (Figure S3). Detailed parameters for CV measurements such as capacitance, dielectric thickness, and gate areas of PVA and PMMA (Table S1) for calculating the dielectric constant. The Supporting Information is available free of charge on the ACS Publications website at DOI: 10.1021/am508996r.

AUTHOR INFORMATION

Corresponding Author

*Tel.: +886 35715131 #42568. Fax: + 886 3 5737406. E-mail: nhtai@mx.nthu.edu.tw.

Notes

The authors declare no competing financial interest.

ACKNOWLEDGMENTS

The authors acknowledge the support from the National Science Council, Taiwan, under Contract 101-2221-E-007-064-MY3.

REFERENCES

(1) Geim, A. K.; Novoselov, K. S. The Rise of Graphene. *Nat. Mater.* **2007**, *6*, 183–191.
(2) Novoselov, K. S.; Geim, A. K.; Morozov, S. V.; Jiang, D.; Katsnelson, M. I.; Grigorieva, I. V.; Dubonos, S. V.; Firsov, A. A. Two-Dimensional Gas of Massless Dirac Fermions in Graphene. *Nature* **2005**, *438*, 197–200.
(3) Lee, C.; Wei, X. D.; Kysar, J. W.; Hone, J. Measurement of the Elastic Properties and Intrinsic Strength of Monolayer Graphene. *Science* **2008**, *321*, 385–388.
(4) Bonaccorso, F.; Sun, Z.; Hasan, T.; Ferrari, A. C. Graphene Photonics and Optoelectronics. *Nat. Photonics* **2010**, *4*, 611–622.
(5) Choi, W.; Lahiri, I.; Seelaboyina, R.; Kang, Y. S. Synthesis of Graphene and Its Applications: A Review. *Crit. Rev. Solid State Mater. Sci.* **2010**, *35*, 52–71.
(6) Liu, H.; Liu, Y.; Zhu, D. Chemical Doping of Graphene. *J. Mater. Chem.* **2011**, *21*, 3335–3345.
(7) Schedin, F.; Geim, A. K.; Morozov, S. V.; Hill, E. W.; Blake, P.; Katsnelson, M. I.; Novoselov, K. S. Detection of Individual Gas Molecules Adsorbed on Graphene. *Nat. Mater.* **2007**, *6*, 652–655.
(8) Giovannetti, G.; Khomyakov, P. A.; Brocks, G.; Karpan, V. M.; van den Brink, J.; Kelly, P. J. Doping Graphene with Metal Contacts. *Phys. Rev. Lett.* **2008**, *101*, 026803.
(9) Guo, B.; Fang, L.; Zhang, B.; Gong, J. R. Graphene Doping: A Review. *Nanotechnology* **2011**, *1*, 80–89.
(10) Wang, H.; Zhou, Y.; Wu, D.; Liao, L.; Zhao, S.; Peng, H.; Liu, Z. Synthesis of Boron-Doped Graphene Monolayers Using the Sole Solid Feedstock by Chemical Vapor Deposition. *Small* **2013**, *9*, 1316–1320.
(11) Wei, D.; Liu, Y.; Wang, Y.; Zhang, H.; Huang, L.; Yu, G. Synthesis of N-Doped Graphene by Chemical Vapor Deposition and Its Electrical Properties. *Nano Lett.* **2009**, *9*, 1752–1758.
(12) Guo, B.; Liu, Q.; Chen, E.; Zhu, H.; Fang, L.; Gong, J. R. Controllable N-Doping of Graphene. *Nano Lett.* **2010**, *10*, 4975–4980.
(13) Yoo, H.; Kim, Y.; Lee, J.; Lee, H.; Yoon, Y.; Kim, G.; Lee, H. n-Type Reduced Graphene Oxide Field-Effect Transistors (FETs) from Photoactive Metal Oxides. *Chem.–Eur. J.* **2012**, *18*, 4923–4929.
(14) Wang, X.; Zhi, L.; Müllen, K. Transparent, Conductive Graphene Electrodes for Dye-Sensitized Solar Cells. *Nano Lett.* **2008**, *8*, 323–327.
(15) Yu, A.; Wu, G.; Zhang, F.; Yang, Y.; Guan, N. Synthesis and Characterization of N-Doped TiO_2 Nanowires with Visible Light Response. *Catal. Lett.* **2009**, *129*, 507–512.
(16) Ho, P.-H.; Yeh, Y.-C.; Wang, D.-Y.; Li, S.-S.; Chen, H.-A.; Chung, Y.-H.; Lin, C.-C.; Wang, W.-H.; Chen, C.-W. Self-Encapsulated Doping of N-Type Graphene Transistors with Extended Air Stability. *ACS Nano* **2012**, *6*, 6215–6221.
(17) Tsai, L. W.; Tai, N. H. Enhancing the Electrical Properties of a Flexible Transparent Graphene-Based Field-Effect Transistor Using Electropolished Copper Foil for Graphene Growth. *ACS Appl. Mater. Interfaces* **2014**, *6*, 10489–10496.
(18) Albrektsen, O.; Eriksen, R. L.; Novikov, S. M.; Schall, D.; Karl, M.; Bozhevolnyi, S. I.; Simonsen, A. C. High Resolution Imaging of Few-Layer Graphene. *J. Appl. Phys.* **2012**, *111*, 064305.
(19) Gupta, A.; Chen, G.; Joshi, P.; Tadigadapa, S.; Eklund, P. C. Raman Scattering from High-Frequency Phonons in Supported N-Graphene Layer Films. *Nano Lett.* **2006**, *6*, 2667–2673.
(20) Nemes-Incze, P.; Osvath, Z.; Kamaras, K.; Biro, L. P. Anomalies in Thickness Measurements of Graphene and Few Layer Graphite

Crystals by Tapping Mode Atomic Force Microscopy. *Carbon* **2008**, *46*, 1435−1442.
(21) Giannazzo, F.; Sonde, S.; Raineri, V.; Patané, G.; Compagnini, G.; Aliotta, F.; Ponterio, R. Rimini, E. Optical, Morphological and Spectroscopic Characterization of Graphene on SiO_2. *Phys. Status Solidi C* **2010**, *7*, 1251−1255.
(22) Mechler, Á.; Kopniczky, J.; Kokavecz, J.; Hoel, A.; Granqvist, C.-G.; Heszler, P. Anomalies in Nanostructure Size Measurements by AFM. *Phys. Rev. B: Condens. Matter Mater. Phys.* **2005**, *72*, 125407.
(23) Ferrari, A. C.; Robertson, J. Interpretation of Raman Spectra of Disordered and Amorphous Carbon. *Phys. Rev. B: Condens. Matter Mater. Phys.* **2000**, *61*, 14095−14107.
(24) Malard, L. M.; Pimenta, M. A.; Dresselhaus, G.; Dresselhaus, M. S. Raman Spectroscopy in Graphene. *Phys. Rep* **2009**, *473*, 51−87.
(25) Ferrari, A. C. Raman spectroscopy of graphene and graphite: Disorder, Electron−Phonon Coupling, Doping and Nonadiabatic Effects. *Solid State Commun.* **2007**, *143*, 47−57.
(26) Wang, Y. Y.; Ni, Z. H.; Yu, T.; Shen, Z. X.; Wang, H. M.; Wu, Y. H.; Chen, W.; Wee, A. T. S. Raman Studies of Monolayer Graphene: The Substrate Effect. *J. Phys. Chem. C* **2008**, *112*, 10637−10640.
(27) Ferrari, A. C.; Meyer, J. C.; Scardaci, V.; Casiraghi, C.; Lazzeri, M.; Mauri, F.; Piscanec, S.; Jiang, D.; Novoselov, K. S.; Roth, S.; Geim, A. K. Raman Spectrum of Graphene and Graphene Layers. *Phys. Rev. Lett.* **2006**, *97*, 187401.
(28) Szafranek, B. N.; Schall, D.; Otto, M.; Neumaier, D.; Kurz, H. High On/Off Ratios in Bilayer Graphene Field Effect Transistors Realized by Surface Dopants. *Nano Lett.* **2011**, *11*, 2640−2643.
(29) Kim, S.; Nah, J.; Jo, I.; Shahrjerdi, D.; Colombo, L.; Yao, Z.; Tutuc, E.; Banerjee, S. K. Realization of a High Mobility Dual-Gated Graphene Field Effect Transistor with Al_2O_3 Dielectric. *Appl. Phys. Lett.* **2009**, *94*, 062107.
(30) Zhang, Z.; Xu, H.; Zhong, H.; Peng, L. M. Direct Extraction of Carrier Mobility in Graphene Field-Effect Transistor Using Current−Voltage and Capacitance−Voltage Measurements. *Appl. Phys. Lett.* **2012**, *101*, 213103.
(31) Kim, B. J.; Jang, H.; Lee, S.-K.; Hong, B. H.; Ahn, J.-H.; Cho, J. H. High-Performance Flexible Graphene Field Effect Transistors with Ion Gel Gate Dielectrics. *Nano Lett.* **2010**, *10*, 3464−3466.
(32) Stevanovic, A.; Büttner, M.; Zhang, Z.; Yates, J. T. Photoluminescence of TiO_2: Effect of UV Light and Adsorbed Molecules on Surface Band Structure. *J. Am. Chem. Soc.* **2012**, *134*, 324−332.
(33) McCreary, K. M.; Pi, K.; Kawakami, R. K. Metallic and Insulating Adsorbates on Graphene. *Appl. Phys. Lett.* **2011**, *98*, 192101.
(34) Newaz, A. K. M.; Puzyrev, Y. S.; Wang, B.; Pantelides, S. T.; Bolotin, K. I. Probing Charge Scattering Mechanisms in Suspended Graphene by Varying Its Dielectric Environment. *Nat. Commun.* **2012**, *3*, 734.
(35) Dean, C. R.; Young, A. F.; Meric, I.; Lee, C.; Wang, L.; Sorgenfrei, S.; Watanabe, K.; Taniguchi, T.; Kim, P.; Shepard, K. L.; Hone, J. Boron Nitride Substrates for High-Quality Graphene Electronics. *Nat. Nanotechnol.* **2010**, *5*, 722−726.
(36) Boyd, D. A.; Lin, W. H.; Hsu, C. C.; Teague, M. L.; Chen, C. C.; Lo, Y. Y.; Chan, W. Y.; Su, W. B.; Cheng, T. C.; Chang, C. S.; Wu, C. I.; Yeh, N. C. Single-Step Deposition of High-Mobility Graphene at Reduced Temperatures. *Nat. Commun.* **2015**, *6*, 6620.
(37) Zomer, P. J.; Dash, S. P.; Tombros, N.; van Wees, B. J. A Transfer Technique for High Mobility Graphene Devices on Commercially Available Hexagonal Boron Nitride. *Appl. Phys. Lett.* **2011**, *99*, 232104.
(38) Tedesco, J. L.; VanMil, B. L.; Myers-Ward, R. L.; McCrate, J. M.; Kitt, S. A.; Campbell, P. M.; Jernigan, G. G.; Culbertson, J. C.; Eddy, C. R.; Gaskill, D. K. Hall Effect Mobility of Epitaxial Graphene Grown on Silicon Carbide. *Appl. Phys. Lett.* **2009**, *95*, 122102.
(39) Chen, F.; Xia, J.; Ferry, D. K.; Tao, N. Ionic Screening of Charged-Impurity Scattering in Graphene. *Nano Lett.* **2009**, *9*, 1621−1625.
(40) Van Dover, R. B. Amorphous Lanthanide-Doped TiO_x Dielectric Films. *Appl. Phys. Lett.* **1999**, *74*, 3041−3043.
(41) Hanaor, D. A. H.; Sorrell, C. C. Review of the Anatase to Rutile Phase Transformation. *J. Mater. Sci.* **2011**, *46*, 855−874.
(42) Zukalova, M.; Prochazka, J.; Bastl, Z.; Duchoslav, J.; Rubacek, L.; Havlicek, D.; Kavan, L. Facile Conversion of Electrospun TiO_2 into Titanium Nitride/Oxynitride Fibers. *Chem. Mater.* **2010**, *22*, 4045−4055.
(43) Kobayakawa, K.; Murakami, Y.; Sato, Y. Visible-Light Active N-Doped TiO_2 Prepared by Heating of Titanium Hydroxide and Urea. *J. Photochem. Photobiol. A* **2005**, *170*, 177−179.
(44) Tsai, M. C.; Tsai, T. L.; Lin, C. T.; Chung, R. J.; Sheu, H. S.; Chiu, H. T.; Lee, C. Y. Tailor Made Mie Scattering Color Filters Made by Size-Tunable Titanium Dioxide Particles. *J. Phys. Chem. C* **2008**, *112*, 2697−2702.
(45) Chen, T. T.; Liu, H. P.; Wei, Y. J.; Chang, I. C.; Yang, M. H.; Lin, Y. S.; Chan, K. L.; Chiu, H. T.; Lee, C. Y. Porous Titanium Oxynitride Sheets as Electrochemical Electrodes for Energy Storage. *Nanoscale* **2014**, *6*, 5106−5109.

DOI: 10.1021/am508996r
ACS Appl. Mater. Interfaces 2015, 7, 9453−9461